JACS
JOURNAL OF THE AMERICAN CHEMICAL SOCIETY
Article
pubs.acs.org/JACS

All The Catalytic Active Sites of MoS_2 for Hydrogen Evolution

Guoqing Li,[†,‡] Du Zhang,[⊥] Qiao Qiao,[▽] Yifei Yu,[†] David Peterson,[§] Abdullah Zafar,[§] Raj Kumar,[†] Stefano Curtarolo,[#] Frank Hunte,[†] Steve Shannon,[§] Yimei Zhu,[▽] Weitao Yang,[⊥] and Linyou Cao*[,†,∥]

[†]Department of Materials Science and Engineering, [‡]College of Textiles, [§]Department of Nuclear Engineering, and [∥]Department of Physics, North Carolina State University, Raleigh, North Carolina 27695, United States

[⊥]Department of Chemistry and [#]Department of Mechanical Engineering and Materials Science, Duke University, Durham, North Carolina 27708, United States

[▽]Department of Condensed Matter Physics and Materials Science, Brookhaven National Laboratory, Upton, New York 11973, United States

Supporting Information

ABSTRACT: MoS_2 presents a promising low-cost catalyst for the hydrogen evolution reaction (HER), but the understanding about its active sites has remained limited. Here we present an unambiguous study of the catalytic activities of all possible reaction sites of MoS_2, including edge sites, sulfur vacancies, and grain boundaries. We demonstrate that, in addition to the well-known catalytically active edge sites, sulfur vacancies provide another major active site for the HER, while the catalytic activity of grain boundaries is much weaker. The intrinsic turnover frequencies (Tafel slopes) of the edge sites, sulfur vacancies, and grain boundaries are estimated to be 7.5 s^{-1} (65−75 mV/dec), 3.2 s^{-1} (65−85 mV/dec), and 0.1 s^{-1} (120−160 mV/dec), respectively. We also demonstrate that the catalytic activity of sulfur vacancies strongly depends on the density of the vacancies and the local crystalline structure in proximity to the vacancies. Unlike edge sites, whose catalytic activity linearly depends on the length, sulfur vacancies show optimal catalytic activities when the vacancy density is in the range of 7−10%, and the number of sulfur vacancies in high crystalline quality MoS_2 is higher than that in low crystalline quality MoS_2, which may be related with the proximity of different local crystalline structures to the vacancies.

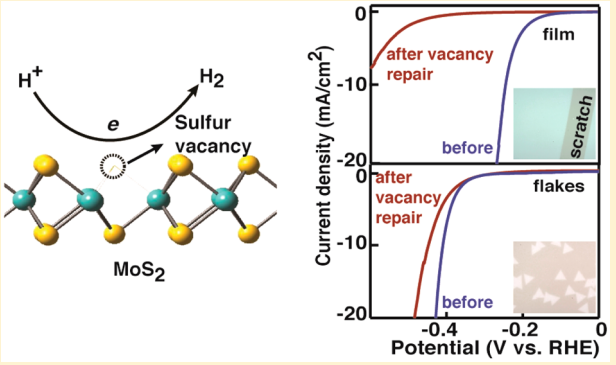

INTRODUCTION

The evolution of hydrogen from water stands as an appealing strategy for energy storage. It may store electrical or solar energy in the format of a chemical fuel (hydrogen) that can be delivered at will and consumed with negligible impact to the environment. However, the implementation of this energy storage strategy has been delayed by the imperfection of the catalysts that are required to drive the reaction. Ideal catalysts would feature high catalytic activities and low cost. Noble metals such as Pt can provide excellent catalytic activities for the hydrogen evolution reaction (HER), but they are too expensive and scarce to be useful for massive application. Molybdenum disulfide (MoS_2) has been considered to be a promising low-cost alternative.[1−3] This material bears particular implications for the storage of solar energy due to its capability to efficiently absorb solar radiation[4,5] and to quickly transfer interfacial charge.[6] Unfortunately, the catalytic activity of MoS_2 is much inferior to that of Pt, and it is necessary to substantially improve the activity for the sake of practical applications.

One key challenge for improving the catalytic activity of MoS_2 is the lack of an unambiguous understanding of its catalytically active sites. The common theory purports only the edge sites of crystalline MoS_2 to be catalytically active, while the basal plane is inert for hydrogen evolution.[7] As a result, one major strategy explored to improve the catalytic activity is increasing the number of edge sites.[8−14] Some recent studies have demonstrated other ways to enhance the catalytic activity of MoS_2 for hydrogen evolution.[15,16] For instance, MoS_2 with the 1T structural phase may show improved catalytic activities, even with substantial oxidation at the edge sites.[17−20] It has also been demonstrated that the catalytic activity of MoS_2 films increases as the thickness decreases and can be even higher than that of edge-rich pyramid MoS_2 nanoplates.[6,21] These results strongly suggest that the catalytic activity of MoS_2 for hydrogen evolution is more complicated that what has been commonly believed.

Here we have unambiguously demonstrated that, besides the edge sites, the sulfur vacancy of MoS_2 provides another major catalytically active site for the HER. The grain boundary may show some catalytic activity as well. The turnover frequency (TOF) of the edge sites, sulfur vacancies, and grain boundaries

Received: June 17, 2016
Published: November 29, 2016

DOI: 10.1021/jacs.6b05940
J. Am. Chem. Soc. 2016, 138, 16632−16638

are quantitatively evaluated to be 7.5 ± 1.5, 3.2 ± 0.4, and around 0.1 s^{-1}, respectively, and the typical Tafel slopes are 65−75, 65−85, and 120−160 mV/dec for the edge sites, sulfur vacancies, and grain boundaries. Unlike the linear dependence on the length of the edge sites and grain boundaries, the catalytic activity shows a maximum with the density of sulfur vacancies in the range of 7−10%. Our result indicates that the catalytic activity of the sulfur vacancies is also related to the crystalline quality close to the vacancies, as higher crystalline quality nearby may enable higher catalytic activity at the vacancies. The desired structure would be monolayer MoS_2 that involves the optimal density of sulfur vacancies and is otherwise highly crystalline in quality. It is worthwhile to point out that a very recent work has also claimed catalytic activities at the sulfur vacancies of MoS_2 for the HER,[22] but the experimental results used to support the claim are misinterpreted and actually cannot support the claim [see section S1 of the Supporting Information (SI)]. In stark contrast with the previous studies,[22] our experimental results indicate that the sulfur vacancies created by Ar plasma treatment are not catalytically active, which is likely due to the proximity of an unfavorable crystalline structure to the plasma-created vacancies.

EXPERIMENTAL SECTION

Synthesis and Transfer of Monolayer MoS_2 Films and Flakes. MoS_2 thin films were synthesized using a self-limiting chemical vapor deposition process that we have recently developed.[23] Briefly, molybdenum chloride ($MoCl_5$) powder (99.99%, Sigma-Aldrich) was placed at the center of a furnace and sulfur powder (Sigma-Aldrich) at the upstream entry of the furnace. Receiving substrates (sapphire) were placed in the downstream of the tube. Typical conditions include a temperature of 850 °C, a flow rate of 50 sccm, and a pressure around 2 Torr. The films with different densities of sulfur vacancies were grown by varying the growth temperature in the range of 700−900 °C. Monolayer MoS_2 flakes were grown using a different chemical vapor deposition (CVD) technique,[6] in which MoO_3 (99.99%, Sigma-Aldrich) instead of $MoCl_5$ was used as the precursor.

The transfer of the monolayers followed a surface energy assisted transfer approach that we developed previously.[24] Briefly, a layer of polystyrene (PS) was spin-coated on the as-grown monolayers. A water droplet was then dropped on the top of the polymer. Due to the different surface energies of the monolayer and the substrate, water molecules could penetrate under the monolayer, resulting in the delamination of the PS-monolayer assembly. We could pick up the polymer/monolayer assembly with tweezers and transfer it to glassy carbon substrates. Finally, PS was removed by rinsing with toluene several times.

Repair of Sulfur Vacancies. Sulfur repair was conducted following a process reported previously.[25] Basically, monolayer MoS_2 was dipped in a solution of 1/15 (volume ratio) (3-mercaptopropyl)-trimethoxysilane (Sigma-Aldrich)/dichloromethane (Sigma-Aldrich) for 48 h in a dry glovebox. The samples were then rinsed thoroughly with dichloromethane and 2-propanol (Sigma-Aldrich), and blown dry with N_2. Finally, the samples were annealed in a flow of Ar (with 5% H_2) at 350 °C for 20 min.

Structure and Composition Characterizations. Raman measurements were carried out by a Horiba xPlora system at an excitation wavelength at 532 nm. AFM measurements were performed with a Veeco Dimension-3000 atomic force microscope. XPS measurements were carried out with an X-ray photoelectron spectroscope (SPECS System with PHOIBOS 150 analyzer using an Mg Kα X-ray source). Annular dark-field (ADF) STEM images and HRTEM images were acquired using an aberration-corrected JEOL JEM-ARM200CF scanning transmission electron microscope operated at 80 kV. ADF images were processed with a deconvolution filter to improve the contrast. Magnetization measurements were performed at 350 K in a Quantum Design MPMS SQUID VSM. The magnetic field was applied in the plane of the samples that were mounted on a diamagnetic quartz sample holder.

Electrochemical Characterizations. The electrochemical characterization was performed in 0.5 M H_2SO_4 using a CH Instrument electrochemical analyzer (model CHI604D) with a saturated calomel reference electrode (SCE). A Pt mesh (2.54 × 2.54 cm) and a graphite rod were used as the counter electrode, and the tested results did not show any difference. Nitrogen gas was bubbled into the electrolyte throughout the experiment. The potential shift of the SCE is calibrated to be −0.262 V vs RHE. Typical electrochemical characterizations of the monolayers were performed using linear sweeping from 0 to −0.5 V (vs RHE) with a scan rate of 5 mV/s. The electrolyte resistance and capacitance of the electrocatalysts were characterized using electrochemical impedance spectroscopy (EIS). The ac impedance is measured within the frequency range from 10^6 to 1 Hz with a perturbation voltage amplitude of 5 mV (typical EIS measurement results can be seen in Figure S1, SI). An equivalent Randles circuit model was fit to the data to determine the system resistance and capacitance. The electrochemical deposition of Cu was performed in 1 M $CuSO_4$ by linearly sweeping from 0 to −0.08 V (vs RHE) with a scan rate of 5 mV/s.

DFT Computation. All computations in this work were performed with the plane-wave software code VASP (Vienna Ab Initio Simulation Package)[26] using the Perdew−Burke−Ernzerhof (PBE) exchange−correlation energy functional[27] with its corresponding pseudopotentials. For the H adsorption on the basal plane, the Mo edge, and 5−7 and 8−4−4 grain boundary sites, the plane wave cutoff was chosen as 480 eV. The Monkhorst−Pack[28] 2 × 1 × 1 *k*-point grid was applied for the geometry optimizations and the 6 × 1 × 1 *k*-point grid for the single-point energy calculations. For the 12−4 grain boundary sites, the plane wave energy cutoff was chosen as 480 eV for the geometry optimizations and 540 eV for the single-point energy calculations. The Monkhorst−Pack 2 × 1 × 1 *k*-point grid was applied for both the geometry optimizations and the single-point energy calculations.

RESULTS AND DISCUSSION

We start with examining the catalytic activities of continuous monolayer MoS_2 films and discrete monolayer MoS_2 flakes, as shown in Figure 1a,b. The film and flakes are synthesized on sapphire substrates and then transferred onto glassy carbon substrates for catalytic characterizations using a surface energy assisted transfer process that we developed (Figure 1a,b).[24] More specifically, the film is grown using a self-limiting CVD process previously developed by our group,[23] and the flakes are synthesized with another CVD process reported in the references.[29] We have previously demonstrated that the crystalline and surface quality of the film and the flakes may be nicely preserved during the transfer process. We have also confirmed that the film is a continuous and highly uniform monolayer with no voids, cracks, and steps (see ref 22 and Figure S2, SI). The film is expected to bear few edge sites due to the structural continuity (Figure 1a). In contrast, the discrete flakes are monolayers 1 μm in size with well-defined edges (Figures 1b and S2, SI). The presence of few edge sites for the film is supported by magnetic measurement. It is well-known that the edge sites of MoS_2 may provide ferromagnetic moments,[30,31] and our magnetic measurement indeed shows a substantial ferromagnetic moment for the flakes but not the film (Figure 1c). According to the common theory,[32] in which only the edge site is catalytically active, one would expect much worse catalytic performance for the film than for the flakes.

In stark contrast with the intuitive expectation, the edgeless monolayer film exhibits much better catalytic activities than the monolayer flakes. Figure 1d,e shows the polarization curves and

DOI: 10.1021/jacs.6b05940
J. Am. Chem. Soc. 2016, 138, 16632−16638

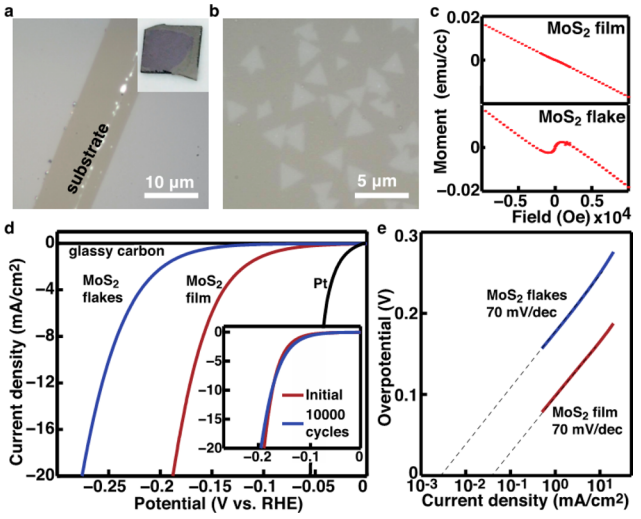

Figure 1. Catalytic activities of continuous monolayer MoS_2 films and discrete monolayer MoS_2 flakes. (a) Optical image of a typical as-grown monolayer MoS_2 film. A scratch is intentionally introduced to show the contrast between the film and the substrate (sapphire). (Inset) Optical image of a typical film transferred onto a glassy carbon substrate around 1 × 1 cm in size. (b) Optical image of discrete monolayer MoS_2 flakes. (c) Magnetic measurement results of monolayer MoS_2 films (upper) and flakes (lower). The straight line indicates the diamagnetic moment of the substrate, and the curved center represents the ferromagnetic moment of the flakes. (d) Polarization curves of monolayer MoS_2 films (blue) and flakes (red). The polarization curves of glass carbon substrates and Pt are also given, as shown. (Inset) Stability test results of monolayer MoS_2 films. The initial result (red) represents the result collected from the film when its performance appears to be stable after pretesting cycles (see Figure S3, SI). (e) Tafel plots derived from the results given in part d. The dashed lines serve to illustrate the Tafel slope and the exchange current density at 0 V overpotential.

corresponding Tafel plots of the film and flakes. The result for the flakes has already been normalized to the area coverage of the flakes on the substrate. The film can provide a current density of 20 mA/cm^2 at an overpotential of around 0.19 V, which is among the best compared to values previously reported with all kinds of MoS_2 materials in the literature.[9−14,17,19,21,33−37] We can find the Tafel slope and exchange current density by fitting the Tafel plots to the equation $\eta = \rho \log(j) + \log(j_0)$, where η is the overpotential (vs RHE), j_0 the exchange current density, and ρ the Tafel slope.[38] Both the film and the flakes show similar Tafel slopes of 70 mV/dec, but the exchange current density of the film is 1 order of magnitude higher, 40 vs 3.5 μA/cm^2 for the flakes. Significantly, the exchange current density of the monolayer film is more than 1 order of magnitude higher than that previously observed for MoS_2 catalysts.[9−14,17,19,21,33−37] This is truly remarkable, as the MoS_2 materials studied in the previous studies often have surface roughness orders of magnitude greater than our atomically smooth film. The capacitance of our smooth film is around 2.6 μF/cm^2, while the capacitance reported in most previous studies are on the scale of several or tens of millifarad. Part of the reason for this extraordinarily high exchange current density is rooted in the atomically thin dimension of the monolayer film. We have previously demonstrated that the exchange current density is dependent on the charge transfer efficiency inside MoS_2, and monolayers can best facilitate the charge transfer in the vertical direction.[6] It is worthwhile to note that the monolayer shows remarkable stability with negligible decrease in the catalytic activity, even after 10 000 cycles.

We find that the catalytic activity of the flakes can be mainly correlated to the edge sites, which is consistent with the common theory. This is evidenced by a linear dependence of the exchange current density of the flakes on the length of edges, as discussed later (see Figure 4d). However, the excellent catalytic activity for the continuous MoS_2 film is unexpected. Previous studies have demonstrated that the catalytic activity of MoS_2 may be substantially improved when its structure is changed from 2H to 1T,[17−19] but we can exclude the possibility of structural changes to be the reason for the high catalytic activity of the film. We examine the Raman (Figure 2a) and

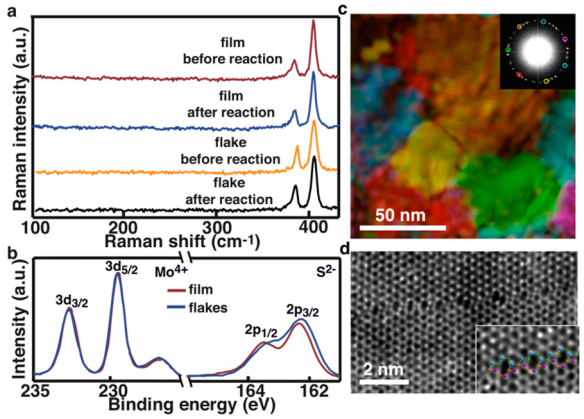

Figure 2. Structural and compositional characterizations of monolayer MoS_2 films and flakes. (a) Raman spectra of monolayer MoS_2 film and flakes before and after the catalytic reaction. The spectra at low wavenumbers are included to indicate no characteristic peaks of 1T MoS_2. (b) XPS results of as-grown MoS_2 film and flakes. (c) False-color dark-field image of the film inverted from the selected spots in the fast Fourier transformation (FFT) pattern (shown in the inset) of original high-resolution TEM (HRTEM) images. A magnified version of the diffraction pattern is given in Figure S5 (SI). Each area with a different color indicates a grain. (d) STEM annular dark-field (ADF) image of a typical grain boundary in the MoS_2 film. The inset shows the 8−4−4 structure at the grain boundary.

XPS (Figure S4, SI) of the monolayers before and after the catalytic reaction and find no change in the composition and crystalline structure of either the film or flakes. Therefore, the unexpected excellent catalytic performance of the edgeless monolayer film strongly suggests the presence of catalytic active sites other than the edge.

To understand the catalytic activity of the film, we examine the possible difference in composition and structure between the film and the flakes. The film is distinguished by the presence of grain boundaries and sulfur vacancies. Unlike the flake, which is well-known to be single crystalline, the film is polycrystalline with a grain size in the range of 30−100 nm (Figure 2c,d). Additionally, XPS measurements show that the stoichiometric ratio of S:Mo in the film is smaller than that of the flakes (Figure 2b), indicating the presence of sulfur vacancies in the film. However, despite the presence of these crystalline defects, the Raman spectrum of the film is similar to that of the flakes, with comparable intensities and line shapes in the two main characteristic Raman peaks A_{1g} and E^1_{2g} (Figure S6, SI). This indicates that the film has an overall high

DOI: 10.1021/jacs.6b05940
J. Am. Chem. Soc. 2016, 138, 16632−16638

crystalline quality but bears some defects, including grain boundaries and sulfur vacancies.

Our experimental result indicates that the catalytic activity of the film can be correlated to the sulfur vacancies. We treated the film and the flakes with a process well-established to repair sulfur vacancies and monitored the catalytic activities before and after the repair.[25,39,40] Briefly, the film and the flake are immersed in (3-mercaptopropyl)trimethoxysilane (MPS), followed by annealing at 300 °C. MPS molecules may be adsorbed at sulfur vacancies and transfer sulfur atoms to the vacancies through the dissociation of S−C bonds under elevated temperature, as illustrated in Figure 3a. The film

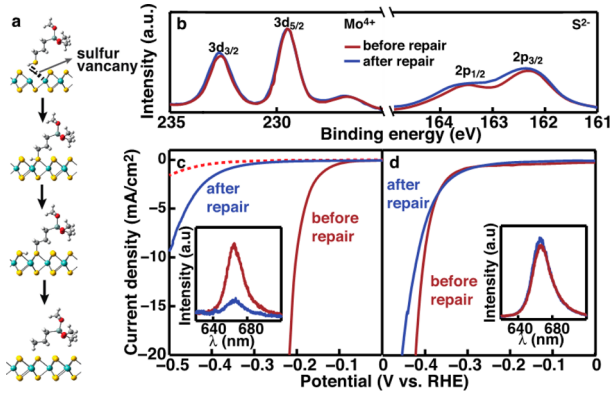

Figure 3. Effect of sulfur vacancy repair on catalytic activity. (a) Schematic illustration for the process of repairing the sulfur vacancies in MoS_2. (b) XPS results of the film before (red) and after (blue) the repair of sulfur vacancies. (c) Polarization curves of the MoS_2 film before (red) and after (blue) the repair of sulfur vacancies. The inset is the PL of the MoS_2 film before (red) and after (blue) the repair. The polarization curve of the flake-merged MoS_2 film with few sulfur vacancies is also given (dashed red). (d) Polarization curves of the MoS_2 flakes before (red) and after (blue) the repair of sulfur vacancies. The inset is the PL of the flakes before (red) and after (blue) the repair.

shows an obvious decrease in photoluminescence (PL) intensity and an increase in the S:Mo stoichiometric ratio after the treatment (Figure 3, part b and the inset of part c), which is consistent with what was reported previously and indicates the successful repair of the sulfur vacancies.[40] In contrast, the flakes show negligible change in PL (Figure 3d inset) and S/Mo ratio (Figure S7, SI) after the treatment, suggesting the presence of few sulfur vacancies in the flakes, as expected. Accordingly, little change can be found in the catalytic performance of the flakes after the repair (Figure 3d), but the catalytic activity of the film dramatically decreases afterward, the exchange current density decreasing by more than 1 order of magnitude from 30.1 to 1 $\mu A/cm^2$ and the Tafel slope increasing from 70 to 125 mV/dec (see the Tafel plots in Figure S8, SI). We can exclude the possible physical covering of residual MPS molecules to be the reason for the decrease in catalytic activity, as it would otherwise give rise to a similar decrease in both film and flakes. The negligible physical coating is also supported by AFM measurements that indicate no obvious change in the thickness of the film after the repair treatment (Figure S9, SI). Therefore, the dramatic decrease in catalytic activity can be ascribed to the elimination of sulfur vacancies by the repair. This indicates that the catalytic activity of the film is mainly contributed by the sulfur vacancies.

Our experimental results also indicate that the catalytic activity of the grain boundaries is weak. This is evidenced by the weak catalytic performance of the film after the repair of sulfur vacancies. With a grain size in the range of 30−100 nm, the film has a considerable amount of grain boundaries. The weak catalytic activity of the grain boundaries is also supported by the poor catalytic performance of the monolayer MoS_2 film with few sulfur vacancies. This vacancy-less film is synthesized with the same process used to grow the flakes and is formed by the merge of neighboring flakes in the case of high nucleation densities. We have confirmed that the flake-merged films have identical composition as the individual flakes with few sulfur vacancies by Raman, PL, and XPS measurements. The flake-merged film also has few edge sites due to its structural continuity, and its grain size is estimated to be around 1 μm. It shows very poor catalytic performance, as indicated by the polarization curve given in Figure 3c (red dashed curve). The exchange current density is as low as 0.04 $\mu A/cm^2$ and the Tafel slope around 160 mV/dec (see the Tafel plot in Figure S9, SI). We find in experiments that the exchange current density of the repaired and flake-merged films shows a roughly linear dependence on the length of the grain boundaries (Figure S10, SI). This further supports that the weak catalytic activities of the repaired and the flake-merged films are mainly contributed by the grain boundaries.

We can quantitatively evaluate the catalytic activity for each of the different sites, including sulfur vacancies, edge sites, and grain boundaries. In order to evaluate the catalytic activity of single sulfur vacancies, we examine the catalytic performance of monolayer MoS_2 films with different densities of sulfur vacancies. The density of sulfur vacancies is controlled by modulating the growth conditions, such as temperature (in the range of 700−900 °C), and may be quantitatively estimated from XPS measurements (Figures 4a and S11, SI). The vacancy density estimated from the XPS measurements is also confirmed by STEM measurements, in which we can directly visualize the sulfur vacancies (Figure S12, SI). We have confirmed that the overall crystalline qualities of all the films are reasonably comparable, as indicated by comparable intensities of the characteristic Raman peaks (Figure S13, SI). Figure 4b shows the polarization curves collected from these films. The catalytic performance is strongly dependent on the vacancy density. To better illustrate the dependence, we extract the exchange current density and Tafel slope from the measured polarization curves and plot them as a function of the vacancy density in Figure 4c. The catalytic activity of the film shows a maximum when the density of sulfur vacancies is in the range of 7−10%, with exchange current densities in the range of 30−60 $\mu A/cm^2$ and Tafel slopes in the range of 65−75 meV/dec. We can estimate the TOF, which indicates the catalytic reaction rate at single active sites, at each sulfur vacancy to be around 3.2 ± 0.4 s^{-1} (see the calculation method in section S2 of the Supporting Information). As a reference, we also study the catalytic performance of the flakes as a function of the density of edge sites. The result indicates a linear dependence of the exchange current density on the edge length per unit area (Figure 4d), which is consistent with what was reported previously.[11,32] We can estimate the turnover frequency of each edge site to be around 7.5 ± 1.5 s^{-1} (see the calculation method in section S2 of the Supporting Information). Additionally, we can roughly estimate that the TOF of each grain boundary site is 0.1 s^{-1} from the result given in Figure S9 (SI), more than 1 or 2 orders of magnitude smaller than that of the sulfur

DOI: 10.1021/jacs.6b05940
J. Am. Chem. Soc. 2016, 138, 16632−16638

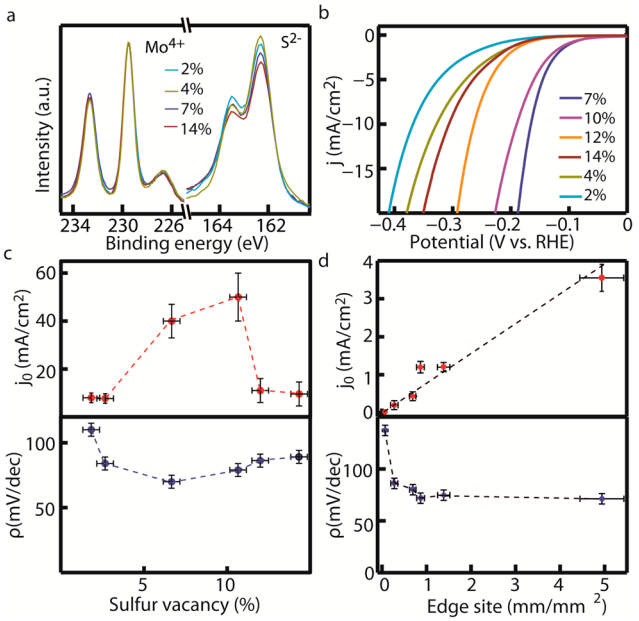

Figure 4. Quantitative evaluation for the catalytic activities of each active site. (a) XPS results for monolayer MoS_2 films with different densities of sulfur vacancies. (b) Polarization curve of the MoS_2 films with different densities of sulfur vacancies. (c) Exchange current densities (upper) and Tafel slopes of the films as a function of the density of sulfur vacancies. The dashed lines serve to guide the eyes. (d) Exchange current densities (upper) and Tafel slopes of the MoS_2 flakes as a function of the edge length per unit area. The dashed lines serve to guide the eyes.

vacancies and edge sites. Unlike the exchange current density, the Tafel slope shows much less dependence on the density of catalytic active sites. The Tafel slope usually remains in the range of 65−75 and 65−85 mV/dec for the edge sites and sulfur vacancies, but it may turn to be much larger when the density of the active sites gets to be very small (Figure 4c,d). The Tafel slope of the grain boundaries is much higher, in the range of 120−160 mV/dec. We do like to point out that the result for the grain boundaries is actually an averaged result over many different types of ground boundaries. In reality, the activity of some grain boundaries could be stronger than others.

We can directly visualize the active sites by performing the electrochemical deposition of Cu metal ($Cu^{2+} \rightarrow Cu^0$) at the MoS_2 film and flakes. The repair of the sulfur vacancies may substantially suppress the Cu deposition on the film but not on the flakes, similar to the effect of the repair on the HER (Figure 3c,d). This indicates that the electrochemical deposition of Cu shares the same catalytically active sites with the HER and can be used to directly visualize the catalytically active sites. Figure 5 shows the Cu particles deposited on the film and the flakes. The Cu particles distribute uniformly everywhere on the MoS_2 film but predominantly at the edge sites for the flakes, which is consistent with our expectation based on the studies of hydrogen evolution. The Cu deposition may also occur at mirror grain boundaries (see Figure 5c and the STEM images of mirror and tilt grain boundaries in Figures S14 and S15, SI), but the deposited particles are obviously smaller and less dense than those deposited at the neighboring edge sites. No Cu deposition can be found at tilt grain boundaries (Figure 5d). This suggests that the mirror grain boundary may have some catalytic activity that is weaker than that of the edge sites, while the tilt grain boundary is not catalytically active.

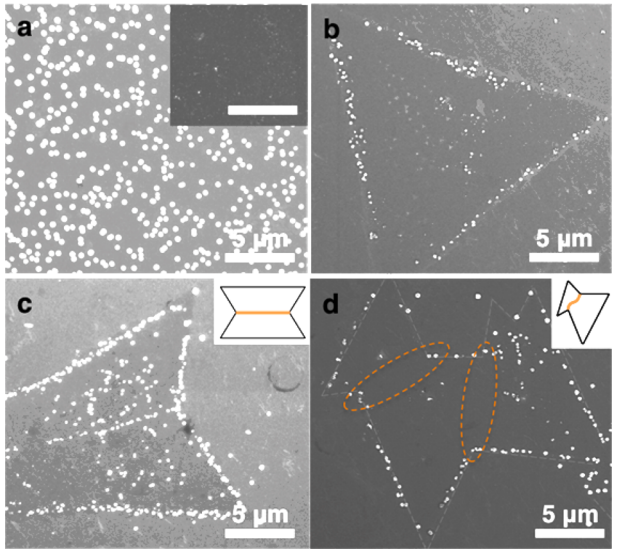

Figure 5. Imaging catalytic active sites with the electrochemical deposition of Cu nanoparticles. (a) SEM images of the Cu particles deposited on MoS_2 films. The inset is the image for the Cu deposition on the MoS_2 film with the sulfur vacancies repaired (scale bar, 10 μm). SEM images of the Cu particles deposited on (b) MoS_2 flakes, (c) MoS_2 flakes with mirror boundaries, and (d) MoS_2 flakes with tilt boundaries. The tilt boundaries are marked with dashed orange ovals. The dashed gray lines in part d mark the edges of the flake. The insets in parts c and d schematically illustrate the mirror and tilt boundaries. More information about the mirror and tilt grain boundaries can be found in Figures S14 and S15.

The experimental result is supported by theoretical calculations. We theoretically examine the adsorption free energy of H atoms, which has been widely considered to be a useful indicator for the catalytic activity, at different sites. Generally, an adsorption free energy closer to zero indicates higher catalytic activities.[41] The calculation results are given in Table 1, and they show reasonable consistency with what was

Table 1. Adsorption Free Energies of H Atoms

sites	ΔG_H^0 (eV)
Mo edge	0.115
S vacancy (1S)	−0.095
grain boundary (8−4−4)	0.181
grain boundary (12−4)	0.368
grain boundary (5−7)	0.566
basal plane	1.218

observed in experiments. The calculation indeed indicates that the Mo edge and sulfur vacancies are the major catalytically active sites. The Mo edge has a hydrogen adsorption free energy of ΔG_H^0 = 0.115 eV, in agreement with previous calculations on the Mo edge of 1H-MoS_2 that also predict small ΔG_H^0. The inertness of the basal plane sites is indicated by the large positive ΔG_H^0 value of 1.218 eV, also corroborated by previously computed results.[42,43] Our computed small ΔG_H^0 values for the two different motifs of S vacancies, in qualitative agreement with the computed results in ref 22, indicate that they also show catalytic activity. This also indicates different catalytic activities at various grain boundaries (see the grain boundary structures in Figures S14 and S15, SI). The 8−4−4 structure, which is involved in the mirror grain boundary, may have some catalytic activity that is weaker than that of the edge

DOI: 10.1021/jacs.6b05940
J. Am. Chem. Soc. 2016, 138, 16632−16638

site and sulfur vacancies, and the other types of grain boundaries, such as 5−7 structures, that are involved in tilt boundaries are much less catalytically active.

As one last note, the catalytic activity of the sulfur vacancies also shows dependence on the local crystalline structure near the vacancy. Generally, the monolayer MoS_2 film with low crystalline quality, as indicated by low Raman and PL intensities, exhibits much worse catalytic activity than the counterpart with comparable sulfur vacancies but higher crystalline quality (Figure S16, SI). With the densities of sulfur vacancies being comparable, the film with lower crystalline quality involves more grain boundaries. The worse catalytic performance suggests that the sulfur vacancies located in or close to grain boundaries are not very active. This observation is consistent with the result of our previous studies. We have previously demonstrated that the monolayer film directly grown on glass carbon substrates, which is in low crystalline quality as indicated by Raman spectra, shows very poor catalytic activity, with the exchange current density being 1 $\mu A/cm^2$ and the Tafel slope of 140 mV/dec.[6] We also find that the sulfur vacancies created by Ar plasma treatment are not catalytically active (see Figures S17−S19, SI). This is likely due to the proximity of unfavorable crystalline structures to the sulfur vacancies, as the plasma treatment may likely also introduce other crystalline imperfections, like Mo vacancies. We believe that the local environment could affect the electronic structure at the sulfur vacancy and eventually affect the catalytic activity. More studies would be necessary to better understand the effect of the local structure close to sulfur vacancies on the catalytic performance.

CONCLUSION

This unambiguous understanding of the catalytically active sites of MoS_2 can provide new insight into the rational design of high-performance MoS_2 HER catalysts. The result indicates that both sulfur vacancies and edge sites may be exploited to improve the catalytic performance of MoS_2, while the grain boundaries may only provide a minor benefit. This explicitly suggests that engineering sulfur vacancies provides a better strategy than increasing the number of edge sites, at least from the perspective of viability. According to the TOF of the sulfur vacancies and the edge sites, to achieve catalytic performance comparable to the films with the optimal range of sulfur vacancies (as reported in Figure 1a) would require a high coverage of well-separated monolayer MoS_2 flakes less than 100 nm in size, the latter of which is very difficult to obtain in experiments. The result also points out that the desired structure would be MoS_2 films with an overall high crystalline quality but involving an optimal density of sulfur vacancies, as the local crystalline structure close to the vacancy may strongly affect the activity of the vacancy. Engineering sulfur defects could be another effective way to enhance the catalytic performance of MoS_2 for hydrogen evolution, besides edge site engineering, phase engineering, and ways to increase electron-hopping efficiency.

ASSOCIATED CONTENT

Supporting Information

The Supporting Information is available free of charge on the ACS Publications website at DOI: 10.1021/jacs.6b05940.

Figures S1−S19; section S1, describing the catalytic inactivity of the sulfur vacancies created by Ar plasma treatment; and section S2, showing the calculation of the turnover frequencies at single active sites (PDF)

AUTHOR INFORMATION

Corresponding Author

*lcao2@ncsu.edu

ORCID

Qiao Qiao: 0000-0002-0229-4407
David Peterson: 0000-0002-4256-9866
Raj Kumar: 0000-0003-4001-0011
Linyou Cao: 0000-0002-7834-8336

Notes

The authors declare no competing financial interest.

ACKNOWLEDGMENTS

This work was supported by CCDM, an EFRC funded by U.S. Department of Energy (DOE), Office of Science, Office of Basic Energy Sciences (BES), under award #DE-SC0012575 (the majority of the experiments, data analysis, and manuscript writing). Y.Z. acknowledges the support by DOE, Office of Science, BES, Materials Sciences and Engineering Division, under contract #DE-SC0012704 (part of the STEM characterization and data analysis). S.S. acknowledges the support of a NSF/DOE partnership in basic plasma science under grant NSF PHY1338917 (the plasma treatment). The authors also acknowledge the use of the Analytical Instrumentation Facility (AIF) at North Carolina State University, which is supported by the State of North Carolina and the National Science Foundation.

REFERENCES

(1) Laursen, A. B.; Kegnaes, S.; Dahl, S.; Chorkendorff, I. *Energy Environ. Sci.* **2012**, *5*, 5577.
(2) Voiry, D.; Yamaguchi, H.; Li, J.; Silva, R.; Alves, D. C. B.; Fujita, T.; Chen, M.; Asefa, T.; Shenoy, V. B.; Eda, G.; Chhowalla, M. *Nat. Mater.* **2013**, *12*, 850.
(3) Merki, D.; Hu, X. L. *Energy Environ. Sci.* **2011**, *4*, 3878.
(4) Huang, L.; Li, G.; Gurarslan, A.; Yu, Y.; Kirste, R.; Guo, W.; Zhao, J.; Collazo, R.; Sitar, Z.; Parsons, G. N.; Kudenov, M.; Cao, L. *ACS Nano* **2016**, *10*, 7493.
(5) Cao, L. *MRS Bull.* **2015**, *40*, 592.
(6) Yu, Y.; Hu, S.; Su, L.; Huang, L.; Liu, Y.; Jin, Z.; Purezky, A. A.; Geohegan, D. B.; Kim, K. W.; Zhang, Y.; et al. *Nano Lett.* **2015**, *15*, 486.
(7) Jaramillo, T. F.; Jørgensen, K. P.; Bonde, J.; Nielsen, J. H.; Horch, S.; Chorkendorff, I. *Science* **2007**, *317*, 100.
(8) Karunadasa, H. I.; Montalvo, E.; Sun, Y. J.; Majda, M.; Long, J. R.; Chang, C. J. *Science* **2012**, *335*, 698.
(9) Kibsgaard, J.; Chen, Z. B.; Reinecke, B. N.; Jaramillo, T. F. *Nat. Mater.* **2012**, *11*, 963.
(10) Kong, D.; Wang, H.; Cha, J. J.; Pasta, M.; Koski, K. J.; Yao, J.; Cui, Y. *Nano Lett.* **2013**, *13*, 1341.
(11) Shi, J. P.; Ma, D. L.; Han, G. F.; Zhang, Y.; Ji, Q. Q.; Gao, T.; Sun, J. Y.; Song, X. J.; Li, C.; Zhang, Y. S.; Lang, X. Y.; Zhang, Y. F.; Liu, Z. F. *ACS Nano* **2014**, *8*, 10196.
(12) Xie, J.; Zhang, J.; Li, S.; Grote, F.; Zhang, X.; Zhang, H.; Wang, R.; Lei, Y.; Pan, B.; Xie, Y. *J. Am. Chem. Soc.* **2013**, *135*, 17881.
(13) Ye, G. L.; Gong, Y. J.; Lin, J. H.; Li, B.; He, Y. M.; Pantelides, S. T.; Zhou, W.; Vajtai, R.; Ajayan, P. M. *Nano Lett.* **2016**, *16*, 1097.
(14) Gao, M. R.; Chan, M. K. Y.; Sun, Y. G. *Nat. Commun.* **2015**, *6*, 78932.
(15) Benck, J. D.; Hellstern, T. R.; Kibsgaard, J.; Chakthranont, P.; Jaramillo, T. F. *ACS Catal.* **2014**, *4*, 3957.
(16) Faber, M. S.; Jin, S. *Energy Environ. Sci.* **2014**, *7*, 3519.

DOI: 10.1021/jacs.6b05940
J. Am. Chem. Soc. 2016, 138, 16632−16638

(17) Voiry, D.; Salehi, M.; Silva, R.; Fujita, T.; Chen, M.; Asefa, T.; Shenoy, V. B.; Eda, G.; Chhowalla, M. *Nano Lett.* **2013**, *13*, 6222.
(18) Lukowski, M. A.; Daniel, A. S.; Meng, F.; Forticaux, A.; Li, L.; Jin, S. *J. Am. Chem. Soc.* **2013**, *135*, 10274.
(19) Wang, H. T.; Lu, Z. Y.; Xu, S. C.; Kong, D. S.; Cha, J. J.; Zheng, G. Y.; Hsu, P. C.; Yan, K.; Bradshaw, D.; Prinz, F. B.; Cui, Y. *Proc. Natl. Acad. Sci. U. S. A.* **2013**, *110*, 19701.
(20) Yin, Y.; Han, J.; Zhang, Y.; Zhang, X.; Xu, P.; Yuan, Q.; Samad, L.; Wang, X.; Wang, Y.; Zhang, Z.; Zhang, P.; Cao, X.; Song, B.; Jin, S. *J. Am. Chem. Soc.* **2016**, *138*, 7965.
(21) Tan, Y. W.; Liu, P.; Chen, L. Y.; Cong, W. T.; Ito, Y.; Han, J. H.; Guo, X. W.; Tang, Z.; Fujita, T.; Hirata, A.; Chen, M. W. *Adv. Mater.* **2014**, *26*, 8023.
(22) Li, H.; Tsai, C.; Koh, A. L.; Cai, L. L.; Contryman, A. W.; Fragapane, A. H.; Zhao, J. H.; Han, H. S.; Manoharan, H. C.; Abild-Pedersen, F.; Norskov, J. K.; Zheng, X. L. *Nat. Mater.* **2016**, *15*, 48−53.
(23) Yu, Y. F.; Li, C.; Liu, Y.; Su, L. Q.; Zhang, Y.; Cao, L. Y. *Sci. Rep.* **2013**, *3*, 1866.
(24) Gurarslan, A.; Yu, Y.; Su, L.; Yu, Y.; Suarez, F.; Yao, S.; Zhu, Y.; Ozturk, M.; Zhang, Y.; Cao, L. *ACS Nano* **2014**, *8*, 11522.
(25) Qiu, H.; Xu, T.; Wang, Z. L.; Ren, W.; Nan, H. Y.; Ni, Z. H.; Chen, Q.; Yuan, S. J.; Miao, F.; Song, F. Q.; Long, G.; Shi, Y.; Sun, L. T.; Wang, J. L.; Wang, X. R. *Nat. Commun.* **2013**, *4*, 2642.
(26) Kresse, G.; Furthmuller, J. *Phys. Rev. B: Condens. Matter Mater. Phys.* **1996**, *54*, 11169.
(27) Perdew, J. P.; Burke, K.; Ernzerhof, M. *Phys. Rev. Lett.* **1996**, *77*, 3865.
(28) Monkhorst, H. J.; Pack, J. D. *Phys. Rev. B* **1976**, *13*, 5188.
(29) Lee, Y. H.; Zhang, X. Q.; Zhang, W. J.; Chang, M. T.; Lin, C. T.; Chang, K. D.; Yu, Y. C.; Wang, J. T. W.; Chang, C. S.; Li, L. J.; Lin, T. W. *Adv. Mater.* **2012**, *24*, 2320.
(30) Tongay, S.; Varnoosfaderani, S. S.; Appleton, B. R.; Wu, J. Q.; Hebard, A. F. *Appl. Phys. Lett.* **2012**, *101*, 123105.
(31) Pan, H.; Zhang, Y. W. *J. Phys. Chem. C* **2012**, *116*, 11752.
(32) Jaramillo, T. F.; Jorgensen, K. P.; Bonde, J.; Nielsen, J. H.; Horch, S.; Chorkendorff, I. *Science* **2007**, *317*, 100.
(33) Benck, J. D.; Chen, Z.; Kuritzky, L. Y.; Forman, A. J.; Jaramillo, T. F. *ACS Catal.* **2012**, *2*, 1916.
(34) Chen, Z. B.; Cummins, D.; Reinecke, B. N.; Clark, E.; Sunkara, M. K.; Jaramillo, T. F. *Nano Lett.* **2011**, *11*, 4168.
(35) Li, Y.; Wang, H.; Xie, L.; Liang, Y.; Hong, G.; Dai, H. *J. Am. Chem. Soc.* **2011**, *133*, 7296.
(36) Li, Y.; Yu, Y.; Huang, Y.; Nielsen, R. A.; Goddard, W. A.; Li, Y.; Cao, L. *ACS Catal.* **2015**, *5*, 448.
(37) Merki, D.; Fierro, S.; Vrubel, H.; Hu, X. L. *Chem. Sci.* **2011**, *2*, 1262.
(38) Bockris, J. O. *Russ. J. Electrochem+* **1995**, *31*, 1211.
(39) Makarova, M.; Okawa, Y.; Aono, M. *J. Phys. Chem. C* **2012**, *116*, 22411.
(40) Cho, K.; Min, M.; Kim, T. Y.; Jeong, H.; Pak, J.; Kim, J. K.; Jang, J.; Yun, S. J.; Lee, Y. H.; Hong, W. K.; Lee, T. *ACS Nano* **2015**, *9*, 8044.
(41) Hinnemann, B.; Moses, P. G.; Bonde, J.; Jorgensen, K. P.; Nielsen, J. H.; Horch, S.; Chorkendorff, I.; Norskov, J. K. *J. Am. Chem. Soc.* **2005**, *127*, 5308.
(42) Tsai, C.; Abild-Pedersen, F.; Nørskov, J. K. *Nano Lett.* **2014**, *14*, 1381.
(43) Tsai, C.; Chan, K.; Abild-Pedersen, F.; Norskov, J. K. *Phys. Chem. Chem. Phys.* **2014**, *16*, 13156.

DOI: 10.1021/jacs.6b05940
J. Am. Chem. Soc. 2016, 138, 16632−16638